Smart Agricultural Technology 8 (2024) 100454

Contents lists available at ScienceDirect

Smart Agricultural Technology

journal homepage: www.journals.elsevier.com/smart-agricultural-technology

A small autonomous field robot for strawberry harvesting

Luis Tituaña [a,*], Akram Gholami [b], Zixuan He [c], Yunjun Xu [a], Manoj Karkee [c], Reza Ehsani [b]

[a] Department of Mechanical and Aerospace Engineering, University of Central Florida, 12760 Pegasus Dr., Orlando, FL, 32816, USA
[b] Department of Mechanical Engineering, University of California, Merced, 5200 N. Lake Rd., Merced, CA, 95343, USA
[c] Department of Biological Systems Engineering, Washington State University, 24106 N. Bunn Rd., Prosser, WA, 99350, USA

ARTICLE INFO

Keywords:
Agricultural robots
YOLO detection
Delta robot
Strawberry harvesting

ABSTRACT

This paper presents the subsystem descriptions and testing of a small robotic platform intended to harvest strawberries that are grown on elevated beds in open field conditions. Agricultural robots can assist in the optimization of farm resources and help solve issues related to increasing farm costs and labor shortages. Monolithic, large size harvesters are already in development; however, they are susceptible to single-point-of-failure and lack the flexibility to adapt to varying field conditions and farm sizes. The proposed robotic harvester covers one row at a time and features a Delta arm configuration manipulator with a five-finger structure as the end-effector to individually pick strawberries. A deep neural network-based vision subsystem using a YOLOv4 model was adopted, which was configured to detect small objects and to locate and classify strawberries into five stages of maturity. During experiments on a commercial farm, the proposed platform, including vision, manipulation, and overbed navigation and control subsystems, achieved an overall success rate of 71.7% for five environment scenarios, with a minimum of 37.5% (the most complicated scenario) and a maximum of 94.0% (the easiest scenario). The average harvesting speed of the system was 7.5 s per strawberry.

1. Introduction

1.1. Urgent needs in agricultural operation automation

The world population is anticipated to reach the 10 billion mark by 2050, which will need an increase of 55% in the current food production to keep up with global caloric demands [1]. According to the 2017 US Census of Agriculture, labor costs in the farming sector increased by approximately 17% with respect to 2012 [2]. Furthermore, increasing labor shortages have been reported in recent years and worsened due to the COVID-19 pandemic [3]. There is a consensus in the agricultural industry that creating labor-saving technologies and enabling agricultural operation automation are keys to protecting producers against the shortage of labor and addressing labor cost issues [4].

Different agricultural robots have been proposed to aid in a variety of farming activities, dealing with varying environments (e.g., lighting, terrain, and weather) and different types of objects (e.g., shape, color, size, distribution, and reflectance) [5]. In spraying, robots precisely deliver the necessary amount of water [6] or pesticide while detecting areas in a farm that require attention [7]. In phenotyping, robots measure physical performance of crops by fusing measurements provided by different onboard sensors [8]. For weeding tasks, robotic systems automatically detect and eliminate weeds in different stages of a crop's growth using mechanical, chemical, fire, laser, or electrical discharge removal methods [9]. Similarly, for pruning tasks, robots detect and selectively remove undesired parts of a plant that would negatively impact its growth [10].

1.2. Background: strawberry harvesting robots and associated subsystem technologies

As of 2017, more than 60,000 acres in the US are dedicated to strawberry production, with a market value of more than 2 billion USD [2]. The states of Florida and California are the largest producers with a combined 76% of total strawberry production in the US [2]. Strawberry harvesting is heavily reliant on manual labor. Thus, the development of a strawberry harvesting robot would greatly reduce their cost and dependence on seasonal workers. Such a machine needs to reliably scout throughout semi-structured strawberry fields, accurately detect

* Corresponding author.
E-mail address: luis.tituana@ucf.edu (L. Tituaña).

https://doi.org/10.1016/j.atech.2024.100454
Received 14 September 2023; Received in revised form 6 April 2024; Accepted 8 April 2024
Available online 12 April 2024

and pick mature strawberries, and maintain a high post-harvest fruit quality.

Strawberry harvesting robots for greenhouses and polytunnels have been extensively studied [11]. In such structured environments, (i) strawberry plants grow in tabletops, allowing pickers to stand upright; and (ii) strawberries hang down to the sides of their pots, mostly uncovered by leaves, making them easier to be detected and picked [12]. In [13], a cable-driven robot is used for harvesting strawberries in polytunnels using a Mitsubishi® 5-DOF serial arm. A new version of this robot is presented in [14] with a single-rail dual-arm manipulator and an obstacle separation algorithm. In [15], a picking mechanism consisting of a movable bench and a stationary 7-DOF robotic arm is designed to approach fruits from below. A Belgium-based company, Octinion, developed the first commercial greenhouse strawberry harvesting robot, Rubion, featuring a robotic arm and a soft end-effector [16].

In contrast, strawberry harvesting robots in open fields have been of less success when compared to their greenhouse counterparts. In open farms, strawberry plants are grown on raised beds. The geometrical dimensions of these beds depend mostly on the type of tractor or machinery used on the farm. These fields are characterized by unstructured growing conditions, with leaves and variable light conditions complicating strawberry detection [17], and sandy or wet terrain creating unfavorable conditions for the motion control subsystem [18]. Nevertheless, several companies are developing robots for strawberry harvesting in open fields. Agrobot, a Spain-based company, created a platform that features 24 robotic arms working in both greenhouses and open fields [19]. Harvest CROO Robotics has developed a harvester that contains 16 picking devices using machine learning algorithms to detect strawberries [20]. Similarly, Advanced Farm Technologies created a mobile platform containing several suction-rotating-picking type robotic arms [21]. Lastly, Traptic developed a system with 8 robotic arms that grab strawberries by their stems [22]. Additionally, while not intended for harvesting, some robots have been designed to aid human pickers. EasyPick, developed by Naber's Ag Equipment LLC, allows workers to lie facing down above the beds to reduce the physical strain of crouching or kneeling [23]. Strawbot, by AgPro Robotics, is a semi-autonomous mobile platform that follows the workers in their harvesting process and collects the picked fruits [24].

Subsystems in strawberry robots have been extensively studied as reviewed in [11]. Aside from the multi-row harvesting configurations, typical designs have a modified version of a tractor, each with its unique capabilities and adapted for working on specific tasks. These include differential steering drive [19] or skid-steered configurations [18,25]. Their navigation subsystems may include GPS, range finders [25], IMU [26], and/or cameras [27,28]. To be able to scout a field, PID algorithms [27], robust controllers [29], and optimal controllers [28] have been successfully applied. Additionally, cooperative configurations of aerial and ground vehicles have been proposed for use in agriculture [30].

When it comes to end-effectors, harvesting robots usually include some sort of suction or cutting mechanism [13] or soft fingers for gripping [31]. An extensive review of agricultural end-effectors for different types of crops can be found in [32]. It has been reported that a maximum force between 22 N [31] and 26 N [15] is enough to detach a strawberry from its stem. Five types of end-effectors have appeared in previous designs [11]: holding-cutting [14], suctioning-pulling [33], suctioning-cutting [34], suctioning [15], and grasping-pulling/twisting [31]. Contact-grabbing end-effectors are common including three-finger claw designs with force limit or fingers assisted with a rotational mechanism to detach from peduncles [31]. The grasping end-effector with force limit sensors [31] is susceptible to fruit orientation inside the fingers. In case of misplacement, a large force is applied that can damage the fruit. The rotational motion to break the strawberry peduncle in [15] is created by tilting the whole harvesting robot arm, which made the harvesting time to be as long as 31.5 s. A different approach is followed in [35] with the design of a spiral-curve tooth to pull strawberries inside a spherical shell.

There are two types of manipulators used in strawberry harvesting: industrial serial arms [13] and rail-based Cartesian type structures [34]. Industrial serial arms are typically expensive, while a Cartesian mechanism, like used in [35], is made up of three perpendicularly oriented linear axes, making it easy to control. However, the operating speeds are slow [35], because some of the moving components must carry motors and other parts, resulting in a more extended period to accelerate or decelerate the inertia of the mechanism.

Aided by the accelerated development of computational hardware and graphical processing units (GPUs), modern machine learning algorithms such as Support Vector Machines (SVM) [36], (Deep) Convolutional Neural Networks (CNN/DCNN) [37], and Region-based Convolutional Neural Networks (R-CNN) [17] were introduced in agricultural applications for fruit identification and maturity grading in open field environments. In [38], RCNN-based networks were applied for agricultural product detection with high accuracy/average precision of over 80% and over 95%, respectively, but the processing speeds of these models were slower than 5 fps, which brought high responding time during the field detection. The above techniques have shown high robustness and accuracy, but their detection speed is limited by the two-stage structure inherent in R-CNN-based models (dense and sparse prediction networks) [39].

A model with promising results for fast detection is the You-Only-Look-Once (YOLO) model [39]. YOLO uses a single feed-forward network that directly outputs bounding boxes and class probabilities, which makes it computationally more efficient than the two-stage models of R-CNNs [39]. Subsequent versions of this model, YOLOv2 [40] and YOLOv3 [41], use anchor boxes and more complex backbone models to improve agricultural products detection performance. YOLOv4 with spatial pyramid pooling (SPP) [42] and path aggregation network (PAN) [43], as discussed in [44], showed promising results with an average precision (AP) of over 90% in detecting mature strawberries with processing speed of ~19 fps based on a field strawberry dataset.

1.3. Focus of this study

The common denominator in current commercial robots is a monolithic robotic platform with multiple arms [19,20]. They work on multiple rows at the same time, allowing harvesting speeds to be comparable to those of a skilled human picker [19,20]. However, such designs have some inherent issues noticeable in the long run: difficult farm-to-farm platform transportation, single-point-of-failure, significant idle time impact, low platform flexibility, and low adjustment capabilities to adapt to field variations [45]. This is the reason a small robotic platform is developed, aiming to cooperatively harvest with similar robots in a fleet in the future, allowing for potentially faster and more robust harvesting when compared to manual harvesting procedures.

In this paper, we present the testing of a modified version of the field robot first shown in [25,27,30], which was intended for disease detection. It is an aluminum structure with a skid steer, differentially driven style [30]. Its navigation system consists of eight ultrasonic range finders that allow scouting over elevated beds, and two quadrature encoders fixed on its drivetrain motors, providing position and velocity feedback [25]. Unlike its predecessor, the robot in this study, shown in Fig. 1, is made of steel, has a fixed height, and a Delta arm configuration manipulator with an actuator to individually pick strawberries. Delta robots are well known in industry for their precision and high speed for picking and placing operations. Their downsides are their high cost and requirement of a high-power source to operate. Our system is developed to defeat these shortcomings while preserving its much-needed accuracy to handle small objects like strawberries. We present a system built with off-the-shelf parts making it easy to build and low-cost. Due to the low weight of strawberries, the load on the arms of the robot is very small and our system can be run with a low-power source (24V). It

Fig. 1. Developed robotic platform.

also has the advantage of being faster than Cartesian mechanisms and many-DOF robotic arms found in the literature. Its small size makes it convenient to transport and allows for the use of multiple arms in a single platform if needed. Moreover, a YOLOv4-based detection system proposed in [44] was adopted and integrated with the robot to identify and spatially locate mature strawberries from RGB images. Also, a harvesting logistic developed for motion control, image processing, and picking is different from its predecessor.

The main contributions of this work are as follows. (i) A robot is experimentally validated, capable of identifying and picking strawberries. (ii) A fast and precise fruit detection model, YOLOv4, was adopted from [44] for detecting and classifying strawberries in their different stages of growth into multiple maturities in field conditions with specific network settings for small objects. (iii) A Delta-arm manipulator is custom-designed to reduce the time in picking. (iv) A high harvesting success rate is achieved. During field experiments, our harvester reached an average success rate of 71.7% including challenging environmental scenarios.

It is worth mentioning that, since the subsystems were designed and developed before the integration, the technologies used therein may not be the most advanced ones. However, the robotic harvesting platform achieves a satisfactory performance during harvesting testing in commercial open fields. Further information about the latest subsystem technology development can be found in published sources from different research groups worldwide. For instance, Zhang et al. [46] developed a strawberry detection algorithm with deep NN using edge devices.

Furthermore, in contrast to the previous strawberry detection software in [44], RGB images with a higher resolution of 768×1152 pixels are fed into YOLOv4, which resulted in more features of strawberry canopies. This allowed the model to detect strawberries in five finely separated maturity levels. This level of strawberry maturity detection in field conditions had not been addressed in the literature yet. Additionally, to achieve a rapid detection of strawberry canopies, the whole detection procedure is simplified as a single YOLOv4 model, while a combination of YOLOv4 and AlexNet was utilized in the previous work [44]. This image processing algorithm was integrated with the robotic harvester, and evaluated in real-time and in-situ under field environment conditions, instead of offline processing based on RGB images presented in [44].

The paper is organized as follows. Section 2 presents three key subsystems: strawberry detection, end-effector/manipulator, and guidance, navigation, and control (GNC). Additionally, the hardware and software will be given. Laboratory and field experiments are presented in Section 3, where failure cases and future directions are also discussed. Finally, in Section 4, conclusions drawn are listed.

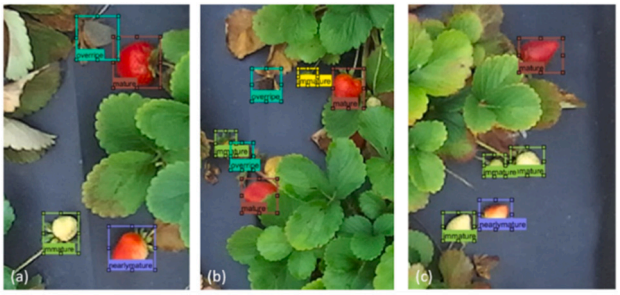

Fig. 2. An example image with the bounding box labels.

2. Materials and methods

2.1. Deep NN-based strawberry detection

2.1.1. Raw image collection and processing [44]

A commercial strawberry farm, located in Oviedo, Florida, was used for collecting images for the training of the strawberry detection model. The sensor used was a ZED 2 camera (RGB-D camera with depth sensing capabilities), from which we acquired RGB images of strawberry plants. Images were collected from February 15 to February 22, 2020. The camera was installed at a fixed height of 100 cm and pointed vertically down onto strawberry beds, and with an average bed height of 30 cm, the distance between the camera and the surface of the beds was 70 cm. A total of 1,400 RGB images were selected and resized to 1000×1200 pixels and the location and maturity (flower, immature, nearly mature, mature, and overripe) of each strawberry in the selected images were manually labeled using labelImg [47] (Fig. 2). More details on the dataset can be found in [44].

2.1.2. Neural network model training

As described in [44], YOLOv4 included three parts: backbone (CSP-Darknet 53), neck (SPP and PAN), and head (structure from YOLOv3) [39] (Fig. 3). The main task of the backbone network (CSPDarknet 53) is to conduct feature generation and image aggregation. The main task of the neck network is to generate the output feature map through the input analysis from the backbone [39]. The head of YOLOv4 was used to apply anchor boxes on the feature map output from its neck and outputs the bounding boxes, probabilities, and label names over the detected targets (i.e., maturity levels of fruits) [39].

The YOLOv4 model first resizes the RGB images to 768×1152 pixels and uses them as inputs. This size of the input layer of YOLOv4 provides sufficient details to extract most of the features in strawberry canopy images. The training strategy, similar to [44], consisted of a total learning iteration of 10,000, and a variable learning rate between 0.001 and 0.00001, as well as 0.949 in momentum and 0.05 in decay. The network settings were changed from the regular/default values to effectively detect small objects in RGB images by following the settings for detection of small objectives in [48].

The training dataset included 1,300 RGB images while the test dataset had 100 images. For comparison, we also trained the YOLOv4 model with images with a 648×768 pixels resolution as in [44]. The performance of models was evaluated by the mean average precision (mAP) and average precision (AP) in each maturity class [44].

2.1.3. Coordinates estimation of detected strawberries

A two-step calibration process is followed to obtain the location of strawberries in the world coordinates, which is defined to be the manipulator's frame of reference. First, a procedure provided by ZED SDK (Colab Inc., 2022) was performed using a calibration board to remove or minimize the effect of lens distortion in RGB images. Second, as shown in Fig. 4, three strawberries (a, b, and c) were placed in fixed locations, and their coordinates $(x_a, y_a), (x_b, y_b)$, and (x_c, y_c) in the manipulator's reference frame were recorded. Using the trained YOLOv4 model, the

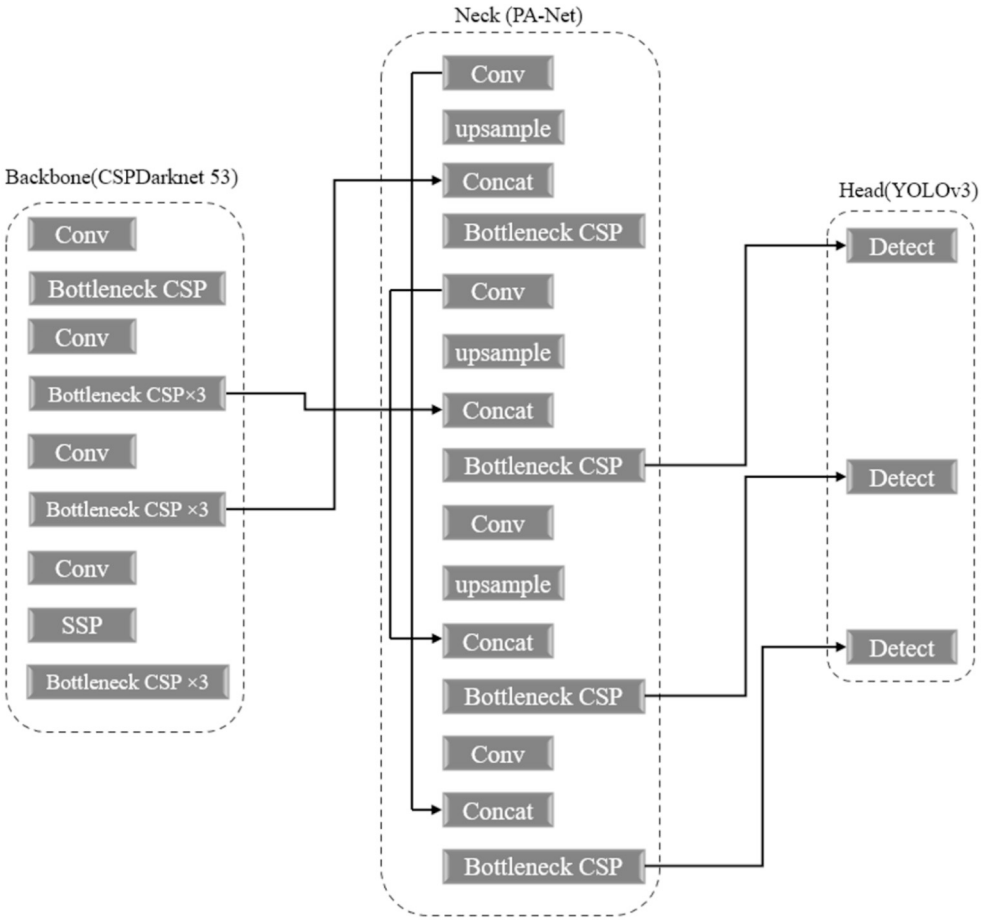

Fig. 3. Architecture of YOLOv4 including backbone (CSPDarknet 53), neck (PA-Net and FPN), and head (YOLOv3), (sketched based on [39]).

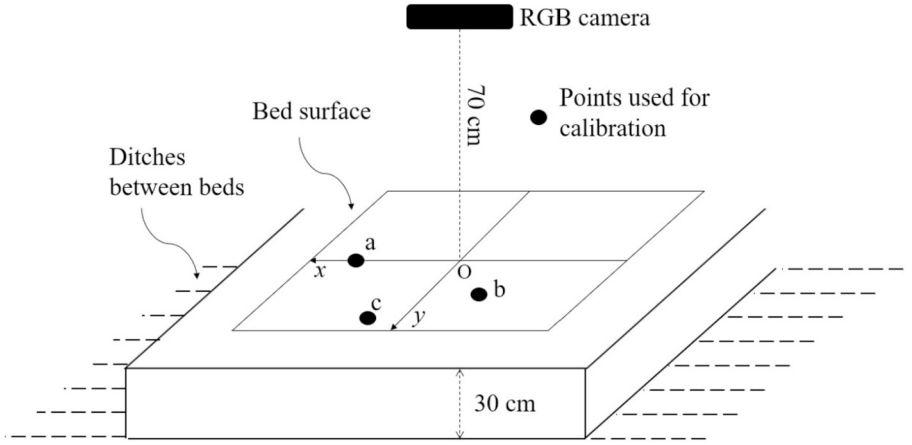

Fig. 4. 2D calibration for estimating strawberry coordinates.

centers $(X_a, Y_a), (X_b, Y_b)$, and (X_c, Y_c) of the bounding boxes covering these three strawberries in the RGB image were detected and recorded, completing the system's calibration process. The location (x_i, y_i) of the ith strawberry in the RGB images and their counterparts (X_i, Y_i) in the manipulator's coordinate frame are linearly related and can be calculated with the following expressions.

$$k_1 = (x_b - x_c)/(X_b - X_c), \tag{1}$$

$$k_2 = (y_a - y_c)/(Y_a - Y_c), \tag{2}$$

$$b_1 = X_a - k_2 x_a = X_b - k_2 x_b = X_c - k_2 x_c, \tag{3}$$

$$b_2 = Y_a - k_2 y_a = Y_b - k_2 y_b = Y_c - k_2 y_c, \tag{4}$$

$$X_i = k_1 x_i + b_1, \tag{5}$$

and,

$$Y_i = k_2 y_i + b_2, \tag{6}$$

where k_1 and k_2 are the slopes, b_1 and b_2 are the intercepts on the x and y axes, respectively, of the target's position in the RGB image coordinates and the 2D/horizontal frame of the robotic manipulator. It is worth mentioning that any of the three equations in Eq. (3) can be used to compute b_1, and the difference between them is very small. Under

field conditions, minor variations in the ground slightly change the camera to bed distance, introducing some error in the estimation of the 2D coordinates (evaluation described in Section 3.4). This error was negligible in practice as we did not observe any issue regarding the motion of the manipulator over detected strawberries. However, a new calibration is always needed if the field conditions are different, and the beds have a different height. For the estimation of the Z-coordinate, we did not use the depth sensing capabilities of the ZED 2 camera. We ask the reader to refer to Remark 6 in Section 3.4 for more details. The height (Z-coordinate) is determined from the origin of the reference frame of the manipulator down to the ground along the negative z-axis. Its estimation is done by using a heuristic method observing that strawberries are located between 70 cm to 72 cm in the field. Starting at 70 cm, the height is increased by 1 cm in each subsequent picking attempt. The reason for this process is explained in Remark 4 in Section 2.6.

Several approaches incorporate the use of LiDAR or its fusion/integration with RGB(D) cameras in fruit detection [49]. However, in our application, incorporating such a sensor would substantially increase the complexity and cost of the vision system with little benefit to the overall performance of the robot. This is because we can easily create an environment with relatively uniform lighting conditions within the workspace of our robot, and strawberries are at a relatively known distance from the camera. Thus, the heuristic method explained before was sufficient for picking strawberries.

2.2. Picking mechanism

2.2.1. Delta arm

The manipulator consists of three arms in a Delta configuration [50], as shown in Fig. 5. The actuators are mounted on the base, reducing the inertia and structural weight of the arms. This arm arrangement allows fast acceleration and high accuracy, suitable for pick-and-place applications [50].

The base of the Delta configuration is connected to three parallel and identical kinematic chains carrying the end-effector. A revolute joint connects each chain to its corresponding four-bar parallelogram link. The chains are made of aluminum, and the joints are 3D printed to keep the structure lightweight. A stepper motor on the base platform actuates each arm, enabling the end-effector to travel along the three Cartesian axes without rotation [51]. The motor drivers are configured to 1,600 micro steps, achieving the resolution of the end-effector movement to be within ± 1 mm. The fixed and moving platform radii are 225 mm and 75 mm, respectively. The active arm length is 250 mm and the forearm length is 520 mm.

2.2.2. Trajectory control

The vision subsystem sends in the target locations of strawberries, which are used to compute the joint angles via an inverse kinematic method [52]. In Fig. 5, the center point of the robotic platform is the origin of the world coordinate frame XYZ. The dimensions of the Delta arm are denoted as r_A, r_B, L_1, L_2, and $\alpha_i, i = 1,2,3$. For a given end-effector coordinate (X, Y, Z), following [52] each active joint angle command is computed with

$$\theta_i = 2\tan^{-1}\left(\frac{-D_i - \sqrt{D_i^2 + E_i^2 - F_i^2}}{F_i - E_i}\right), i = 1,2,3, \tag{7}$$

where,

$$\begin{aligned} D_i &= 2L_1 Z \\ E_i &= 2(r_A - r_B)L_1 - 2L_1 X\cos\alpha_i - 2L_1 Y\sin\alpha_i \\ F_i &= (r_A - r_B)^2 - 2(r_A - r_B)X\cos\alpha_i - 2(r_A - r_B)Y\sin\alpha_i + \\ &\quad L_1^2 - L_2^2 + X^2 + Y^2 + Z^2. \end{aligned} \tag{8}$$

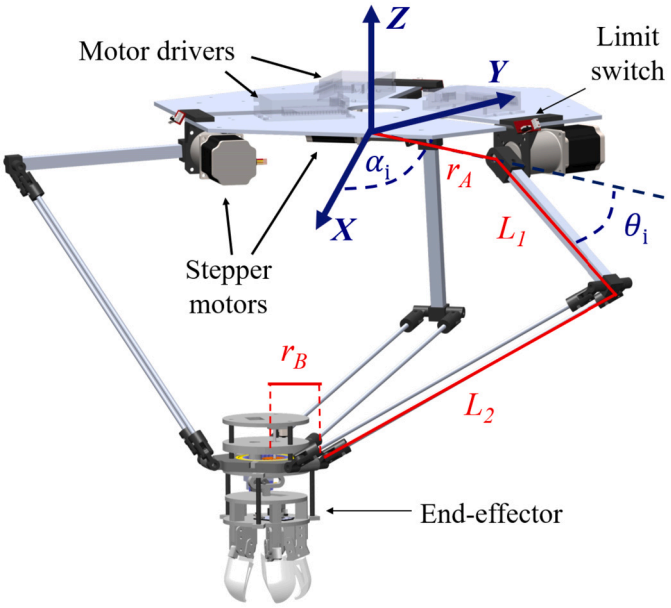

Fig. 5. Schematic view of the developed Delta robot strawberry harvesting manipulator with parameters and geometric relations.

A controller then drives the stepper motors to follow the active joint angle commands computed above. The real-time active joint angles are measured using encoders. The closed-loop system is shown in Fig. 6.

2.2.3. End-effector

The end-effector needs to be robust to the size, position, and orientation of strawberries, and should not damage either plants or fruits [53]. It consists of five identical fingers to grasp the fruit, and a wrist that can rotate about the roll axis to detach it, as shown in Fig. 7(a). Multiple fingers help distribute the holding force around the fruits to reduce bruising. The fingers are flatter towards their tips to try to pull strawberries from below and not squeeze them. Its overall dimensions are 100 mm × 100 mm × 200 mm as shown in Fig. 7. Each finger is part of a four-bar linkage mechanism as described before. These fingers are all connected to a driving translational joint to open or close. The translational movement is created using a single servo motor. The maximum diameter of the end-effector when open is 60 mm, enough to grasp average-sized strawberries between 30 mm and 40 mm [13]. The fingers are 3D printed with hard polylactic acid (PLA) to distribute the holding force around the fruit, and they enclose strawberries almost completely to help prevent their slipping through the sides.

Remark 1. (rotation motion of the end-effector): A rotation mechanism, mimicking human workers, is included in the end-effector, although it was only used in laboratory experiments. As shown in Fig. 7(a), this rotation motion is available to the fingers by gear transmission. In field conditions, when encountered with dense groups of plants, the fingers would grab not only the fruits but also stems and/or nearby fruits. The rotation motion would then spin everything with it changing the location of those initially detected fruits. This is detrimental to the performance of the picking mechanism since a new image is needed after every picking attempt to estimate the new locations of the fruits, increasing the harvesting time.

Remark 2. (eye-in-hand camera): An eye-in-hand Pixy2® camera has been incorporated (Fig. 7(b)) to check if a strawberry is inside the fingers or help the detection of fruits by counting the number of red pixels in an image, similar to [35]. However, we did not use this function in field experiments. When picking a strawberry, stems and leaves would cover the camera lens rendering it useless for any detection task inside

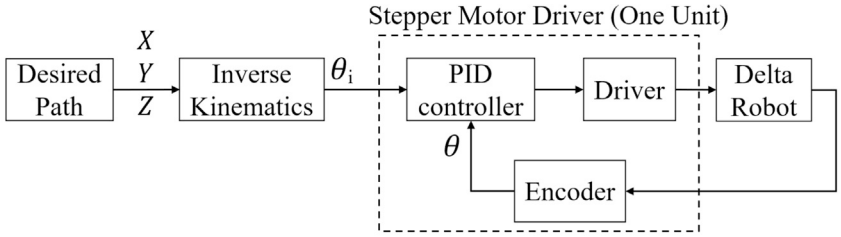

Fig. 6. Block diagram of the picking mechanism trajectory tracking control subsystem.

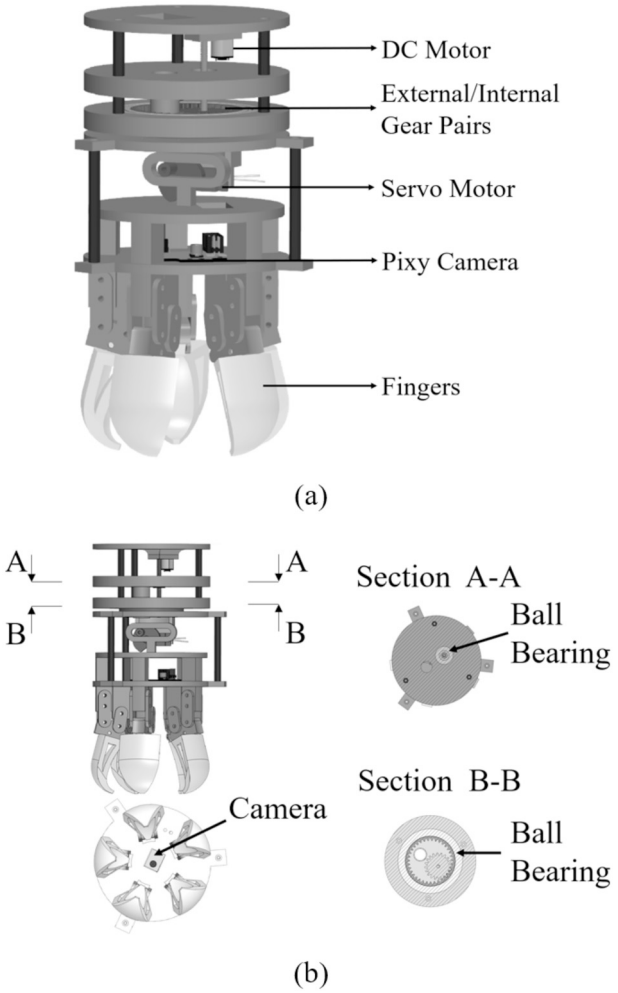

Fig. 7. Schematic view of the developed rotating-grasping end-effector. (a) Isometric view, and (b) section view.

the fingers. Using the camera to automatically detect strawberries inside the fingers was unreliable as occlusions would produce many false positives and negatives. Instead, we manually counted the times the end-effector picked a strawberry in field experiments.

Remark 3. (Soft material for the fingers): The use of soft materials for the fabrication of the fingers was considered and successfully tested in laboratory conditions on a few plants on pots. However, in field experiments, they proved to be too soft, and strawberries would slip through. Strawberries on the farm seemed to have stronger stems, thus, making them more difficult to detach. As a solution, the hard PLA material we used worked very well but was prone to produce fruit damage. To try to counter this, we designed the fingers flatter towards their tips. In this way, they would go under the fruits as the fingers close and avoid squeezing them.

2.3. Guidance, navigation, and control

GNC enables the harvesting robot to scout throughout a strawberry field without scratching its plastic mulch, precisely move over strawberry beds (over-bed), pause at predefined harvesting stops, and rapidly transit at headlands (or cross-bed).

The harvesting robot in this study uses the same GNC subsystem in the previous version [27–29], meaning that the robot motion is guided by a sequence of two-phase paths: over-bed and headland transition. In the over-bed phase [29], the robot moves forward one distance unit equal to the width of the reachable area of the manipulator on the beds' surface, harvests detected strawberries and moves forward again. In the headland transition, the robot makes a turn, aligns with the row next to it, and moves onto that row [28].

The sensors used here are the same as those in [18,27–30]. In the over-bed motion, ultrasonic range finders are used to align the robot with the strawberry beds and not damage the plastic mulch [29]. In the headland transitions, only RGB cameras are used [27,29].

While in an over-bed phase, the robot is driven by a PID controller according to the computed heading angle error and the mismatch between the bed centerline and the robot's center of mass [29]. Different control strategies have been designed and implemented on row headline transitions. The controller here utilizes a search-space dimension reduced dynamic programming-based optimal control method in headline transitions [28]. The onboard camera automatically tunes its brightness and shutter speed [27]. As shown in [28], the over-bed and headline transitions reach the centimeter level of accuracy.

2.4. Hardware integration

As shown in Fig. 8, the hardware architecture of the robot is modified and enhanced based on the previous version in [30], featuring the following major differences. (i) A printed circuit board (PCB) is made to simplify and better organize the circuitry for onboard sensors and actuators. (ii) A Delta manipulator and a finger-type end-effector are designed for strawberry picking. (iii) A YOLOv4 model-based vision processing algorithm is included and tested for fruit detection in field experiments.

An onboard laptop oversees the operation logic of all the subsystems such as drivetrain, GNC, picking, and image processing. GNC relies on information from eight ultrasonic range finders that help the robot remain centered over a bed during its overbed motion [30]. The distance traveled by the robot is obtained from a Kangaroo® motion controller that uses feedback signals from two quadrature encoders attached to the motors, maintaining a given speed set by the GNC algorithm [29]. RGB cameras and row markers are used for row transition (cross-bed) motion [27,28]. Each motor is driven by a Sabertooth® DC motor driver connected to a 12 V battery [30]. The YOLOv4 model-based vision subsystem uses an RGB camera directly connected to the laptop via USB. The Delta manipulator and end-effector are controlled by a Raspberry Pi® and stepper motor drivers. The motion of the manipulator's arms is restricted by three limit switches. The end-effector uses a servo motor to open and close its five fingers. The stepper motors and Raspberry Pi® use a 19 V and 5 V power source, respectively, obtained from DC-DC converters powered by a 12 V battery. A voltage adapter (5 V to 3.3

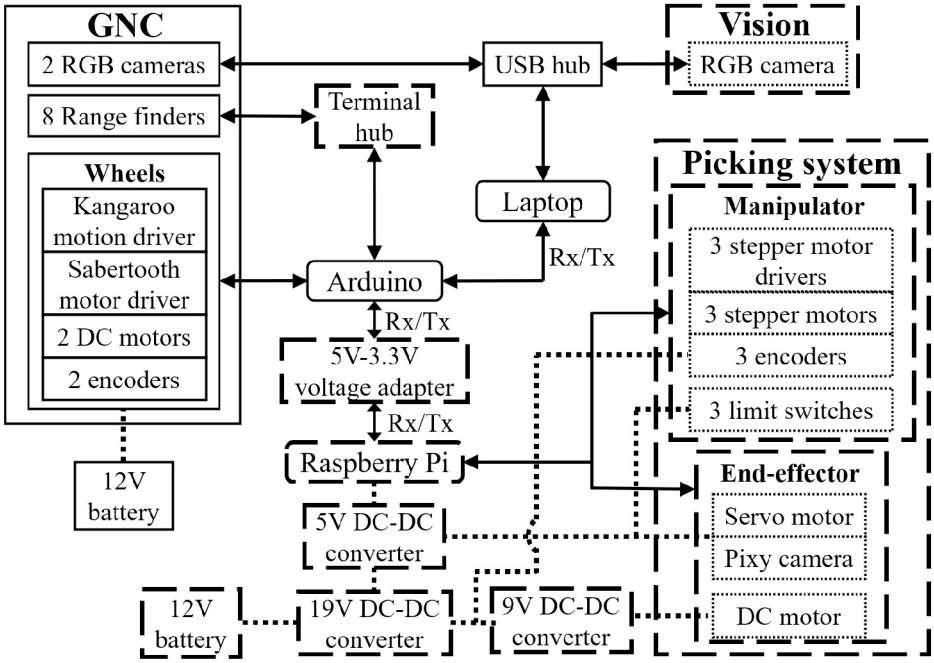

Fig. 8. Hardware architecture. New hardware in the dashed-line boxes.

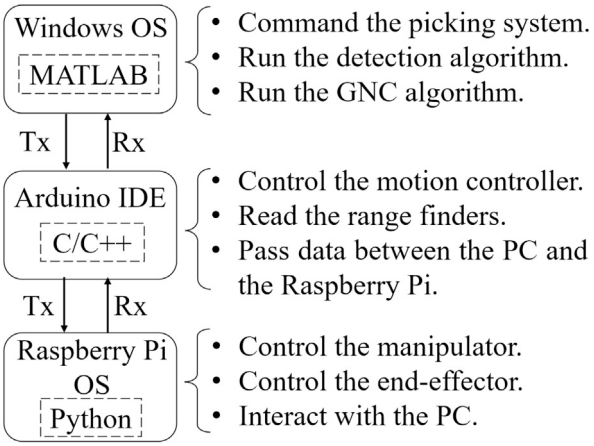

Fig. 9. Software architecture.

V) is used for serial communication between the Arduino and the Raspberry Pi. The new PCB is connected to the Raspberry Pi and contains the voltage regulators to power the stepper motor drivers, DC motor, and servo motor. It also contains a set of terminals to facilitate the transmission of the control signals for the manipulator and the end-effector.

2.5. Software integration

As shown in Fig. 9, three programming languages are used for controlling the robot: MATLAB, C/C++, and Python. The software packages in MATLAB and C/C++ for GNC are from the previous version [30]. We chose these three languages due to their vast community support and their versatility to handle algorithms, sensors, and peripherals from different manufacturers. The laptop runs MATLAB scripts for image processing, strawberry detection, and GNC, and interacts with the manipulator/end-effector. The Arduino MEGA runs a program written in C/C++ to collect information from the ultrasonic range finders and to drive the robot's wheels through the Kangaroo® motion controller [30]. It also allows data transfer between the Raspberry Pi® and the laptop via serial communication. The Raspberry Pi runs a script written in Python to control the manipulator and end-effector, and exchanges information about the picking process with the laptop.

2.6. Control and harvesting sequence

The robot stops every time a picking process starts, which has been termed static harvesting [54]. The control sequence that the robot follows is shown in Fig. 10. After loading the NN parameters and having established the communication with the Arduino and Raspberry Pi, the robot starts to move forward a distance equal to the width of its manipulator's reachable area, which for the Delta configuration is about 50 cm. The robot comes to a stop and takes an image of the bed lying underneath. The vision subsystem passes the coordinates (X, Y, Z) of reachable mature strawberries to the Raspberry Pi to proceed with the picking process (Fig. 11). This process will repeat after three picking attempts have been carried out or until one of the following events happens: the collection basket is full, the robot needs servicing, the end of a row is reached, or all the beds have been harvested. If no mature strawberries are within range, the robot will move forward another 50 cm. Ultimately, the robot will return to a central station where it can charge its batteries or simply be stored for future use.

The picking process (Fig. 11) begins when the locations of reachable mature strawberries are received by the Raspberry Pi. Then, the trajectory paths are calculated using the inverse kinematic method as discussed in Section 2.2. Starting at the home position and with the end-effector's fingers open, the manipulator will move 10 cm down and then parallel to the ground to the first strawberry location. Once over the desired target, the manipulator will move down the remaining distance to match the estimated height. The height will increase by 1 cm each attempt, starting at 70 cm, as described in Section 2.1.3. The fingers are then commanded to close, and the end-effector retracts first 15 cm at a slow speed (~2.9 cm/s) and then 5 cm at a normal speed (~9.3 cm/s). The slow-motion allows the fingers to completely close and grab a strawberry when the height has been overestimated. The retraction action will detach most strawberries from their stem.

Next, the manipulator moves parallel to the ground to the collection basket, the fingers are opened to release the strawberry, and one attempted strawberry is counted. This information is sent to the laptop. If more than one strawberry is within reach, the manipulator will proceed to attempt to pick the next target fruit without going back to the

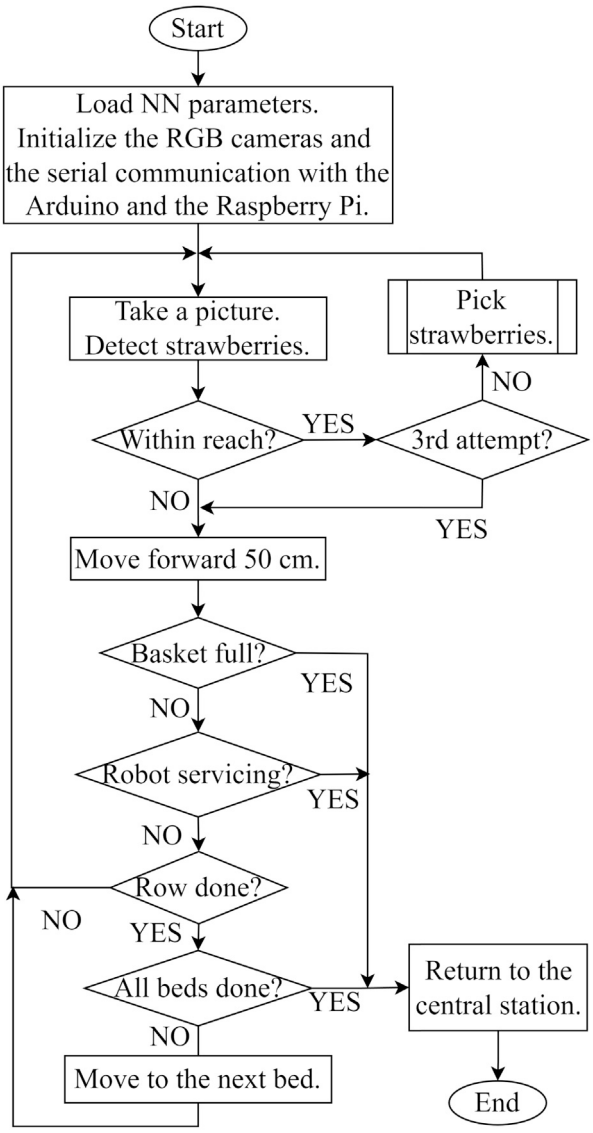

Fig. 10. Flow diagram of the general harvesting process.

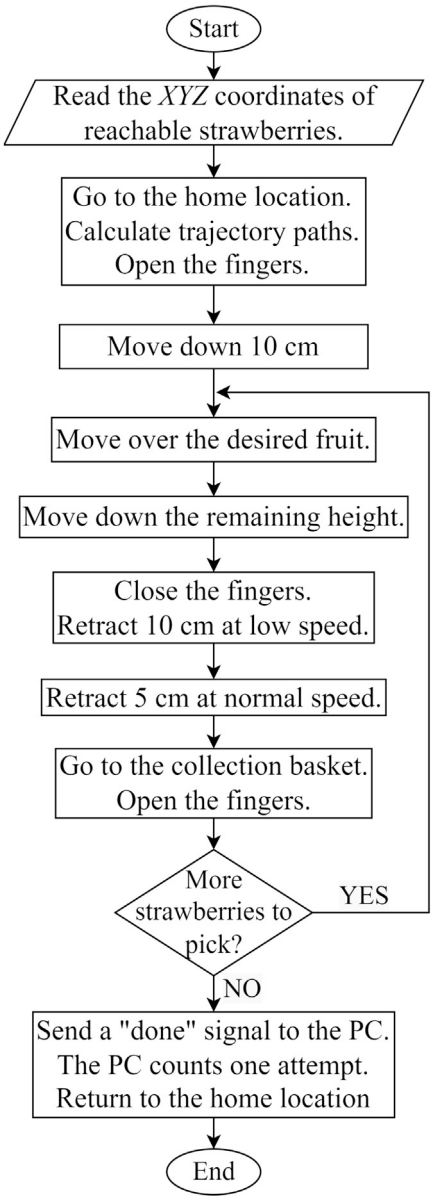

Fig. 11. Flow diagram of the strawberry picking subprocess.

home position. After attempting to pick all reachable strawberries, a "done" signal is sent to the laptop, the manipulator returns to the home position, and one attempt is counted. Another image is taken to update the locations of strawberries that were not picked or might have moved due to previous picking actions. This process is repeated on every bed location up to three times (attempts) or until there are no mature strawberries within reach. If the computer does not receive any information from the Raspberry Pi within a specific amount of time, a timeout scenario is triggered, indicating that either a new picture must be taken, or the robot should move forward.

Remark 4. (height estimation): The height estimation technique previously described resulted to work significantly better than estimating the height using stereoscopic vision, whose accuracy decreases as strawberries are further away from the center of an image. Plus, the same strawberry needed to be detected in both pictures, which is not always the case due to the slight change of perspective of the cameras.

3. Results and discussion

In this section, we first present the laboratory experiments of each of the three subsystems described in Section 2. Then the strawberry picking field experiments conducted on a commercial, open strawberry field are discussed.

3.1. Strawberry detection subsystem evaluation

An example of the output generated by the YOLOv4 model is shown in Fig. 12. Table 1 shows a summary of the performance metrics of the YOLOv4 model in [44] and our modified version. The mAP of YOLOv4 (small objects) with input images that have a resolution of 768×1152 pixels was 89.3% on the training dataset and 80.2% on the test dataset, respectively. These results were slightly better than the mAP of 87.1% on the training dataset and 79.9% on the test dataset achieved by YOLOv4 in the previous work [44]. The detection of mature strawberries, which was the most important target for robotic picking, achieved the highest AP of 91.9% with the test dataset. The trained YOLOv4 in this study also performed well with the immature and nearly mature classes, with an AP of 87.0% and 81.6%, respectively. It shows that the adopted method could distinguish among key maturity stages (immature/nearly mature/mature) of strawberries. Flowers and overripe strawberries were more challenging to detect than the shapes of

Table 1
Performance of the YOLOv4 models in strawberry detection - training and tests datasets.

Datasets	Methods	Image resolution (pixels)	AP of Class (%)					mAP (%)	Processing time (ms)[a]
			Flower	Immature	Nearly mature	Mature	Overripe		
Training (1300 images)	YOLOv4 in [44]	648x768	77.49	91.68	90.20	94.63	81.66	87.13	-
	Ours	768x1152	79.93	92.86	92.55	95.69	85.58	89.32	-
Test (100 images)	YOLOv4 in [44]	648x768	71.51	87.57	81.33	90.31	68.88	79.92	55.19
	Ours	768x1152	69.95	87.02	81.75	91.89	70.41	80.20	64.40

[a] Processing time is achieved using a dedicated GPU.

Table 2
Results of strawberry harvesting mock-up test in the laboratory.

# of target fruits in six different trials	Grasp success	Harvest success	Average harvesting attempts
9	100%	77.7%	1.3
6	83.3%	83.3%	1.0
5	80%	60%	1.4
5	100%	80%	1.2
3	100%	100%	1.0
5	80%	80%	1.2

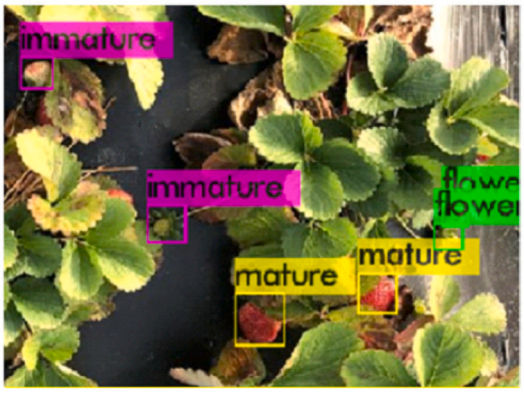

Fig. 12. An example image with strawberries detected by the YOLOv4 model (small objects).

strawberries in the other three groups, which explains the inferior performance of the trained YOLOv4 model when detecting objects in these two groups. The processing time of the new model increased by 9.21 ms when detecting strawberries with higher-resolution images. However, the increase in the processing time is negligible when compared to the overall harvesting time (discussed in Section 3.4). Overall, YOLOv4 (small objects) showed an improved ability in detecting strawberries with different maturity levels, especially mature strawberries when the input image resolution was set to 768×1152 instead of 648×768 used in [44].

3.2. Guidance, navigation and control subsystem evaluation

The GNC subsystem uses the same control strategy as our previous version [29]. Here, we re-tuned the PID controller for the overbed motion to accommodate the larger dimensions of the new robot. The robot is kept centered on the bed with the aid of eight ultrasonic rangefinders that collectively estimate the distance between the center of the robot mass to the row edge. The detailed GNC performance can be found in [28] and [29].

3.3. Picking mechanism subsystem evaluation

Four quantitative performance criteria are selected to evaluate the performance of the picking subsystem: grasp success (%), harvest success (%), average harvesting attempts, and harvesting time (s). We define the grasp success as the number of strawberries that were successfully grabbed (not detached) per target fruit and the harvest success as the number of strawberries detached from the plants per target fruit. In the laboratory experiments, the in-hand camera can detect strawberries inside the fingers by counting the number of red pixels in the image. If no strawberries are detected after the fingers close, the end-effector will open again and attempt to harvest the same fruit in the same location one more time, up to two attempts. Artificial strawberries were placed randomly on a black surface. The results of the laboratory experiments are shown in Table 2. On average, the picking mechanism was 90.9% successful in grasping and 78.8% successful in harvesting the strawberries. The manipulator could harvest single strawberries mostly in one attempt. The two main reasons for failure in laboratory testing are: (i) the artificial strawberries are light; thus, with a minimal touch, they might displace; and (ii) the artificial strawberries are not attached to the experiment surface, so after gripping the fruit, there is a great chance the leaves are facing the in-hand camera; hence, the red pixels cannot be detected, and the end-effector drops the fruit. Please note that the harvesting time in the laboratory experiments is reported in Fig. 17.

3.4. Field experiments

As shown in Fig. 13, field experiments were carried out on a farm where strawberries are grown in open field conditions on elevated beds covered with a black plastic mulch. It is demonstrated in our field experiments that operating the robot is not difficult. Nevertheless, as mentioned in Section 2.1.3, a key step that is always needed upon startup is the camera calibration. To better fit real field conditions, some steps discussed in the control sequence are modified or further explained in the remarks below.

Remark 5. (Impact of the robot's size on the field): Unlike common agricultural machinery like tractors, which are heavy and powered by fossil fuels, the light weight of our robot and its electric power source reduce soil compaction and incurs in significantly lower carbon and nitrogen emissions responsible for soil acidification [55].

Remark 6. (image processing in field conditions): A graphics card is not available in our field setup as it was in our laboratory tests, and without it, the processing time of each image is considerably increased from 55.19 ms to an average of 6.4 s. This is explained by the significantly less processing power of our laptop's CPU when compared to the GPU

Table 3
Strawberry harvesting results in field conditions.

	Type 1 Isolated and mostly uncovered	Type 2 closely grouped, uncovered mature strawberries	Type 3 Isolated and partially covered	Type 4 Loosely grouped, partially covered with obstacles	Type 5 Closely grouped, partially covered with obstacles
1st time	77.50%	46.55%	54.20%	35.48%	13.89%
2nd time	12.00%	34.48%	20.61%	18.28%	15.97%
3rd time	4.50%	3.45%	3.82%	5.38%	7.64%
# Picked	188	49	103	55	54
Total # strawberries	200	58	131	93	144
Success rate	94.00%	84.48%	78.63%	59.14%	37.50%

Fig. 13. Harvesting robot in a nearby commercial, open strawberry field.

used for Deep NN operations. Additionally, without the GPU we were unable to use the depth-sensing capabilities of our RGB-D camera, and instead, we used the method explained in Section 2.6. for height estimation. As noted in this section, the harvesting rate was not impacted significantly by this method, which proved that the use of a depth sensor was not essential.

Remark 7. (light conditions): Natural light on a sunny day intensifies the brightness in images giving strawberries a false color, as shown in Fig. 14. This results in strawberries not being accurately detected or misclassified. However, this negative effect was successfully mitigated by enclosing the robot with a tarp, blocking most of the direct sunlight into the camera's field of view.

Remark 8. (diseased/wilted leaves effects): Diseased and/or wilted leaves were sometimes identified as mature strawberries as their shape, size and color can resemble a mature fruit, as shown in Fig. 15. Out of 655 mature strawberries detected by the vision system, 29 were leaves that will not be counted. This corresponds to a 95.6% accuracy of our YOLOv4 model in the detection of mature strawberries in the field experiments, which is higher than the 91.89% accuracy reported for the trained model on the test dataset in Table 1. Nevertheless, the false positives do not affect the harvesting process as the leaves are only lifted by the end-effector.

Five experiments were conducted throughout March and April 2022, on sunny days from 11 A.M. to 3 P.M. This time of the year is the end of the strawberry season in Florida and plants were in their late stages of development with many wilted leaves and mature/overripe fruits, a challenging time for robotic harvesting. As mentioned in Remark 7, the sides of the robot were covered to decrease the brightness of the images and reduce false positives and negatives in the detection process. Wet terrain due to heavy rain before the day of harvesting did not affect any of our subsystems. The size and tread of our tires are large enough to navigate over mud or sand, and the automatic brightness adjustment of the camera was enough to compensate for dimmer light conditions due to cloudy weather.

To assess the overall picking performance of the robot in the open field, we classified strawberry growth conditions according to their harvesting complexity into five categories (Fig. 16), from Type 1 to Type 5. The classification method is similar to the one in [14] which is meant for strawberries in greenhouses. However, we considered larger groups of mature strawberries as opposed to groups of only one or two fruits in [14]. Furthermore, we have specified a distance between each fruit within each Type. The five classifications are defined as follows:

Type 1: Isolated and mostly uncovered Strawberries are easily identifiable and are not surrounded by leaves, stems, or other fruits. The distance between neighboring strawberries is larger than the size of a typical strawberry.

Type 2: Closely grouped and mostly uncovered Strawberries are mostly uncovered, but found in groups very close to each other, or even touching others.

Type 3: Isolated and partially covered Strawberries seem to be isolated but are somewhat difficult to identify due to leaves partially covering them, making the detection of their centers difficult. The distance between neighboring strawberries is larger than the size of a typical strawberry.

Type 4: Loosely grouped, partially covered with obstacles Strawberries are found in groups but not too close to each other. Leaves are covering some of the groups and stems may be in the way of the gripper. The distance between neighboring strawberries is less than the size of a typical strawberry but are not touching each other.

Type 5: Closely grouped, partially covered with obstacles Strawberries are in groups close to each other. Stems and leaves are on the way of the gripper to reach a strawberry. Neighboring strawberries are touching each other.

Unlike the laboratory tests, two quantitative criteria are selected to evaluate the overall operation performance under field conditions: success rate (%) and harvest time (s). The data shown in Table 3 were manually collected and organized in their corresponding types. Our robot achieved an overall success rate of 71.7% and harvested a total of 626 strawberries in at most three attempts. The success rate drops as more complex the scenario is, with the highest success rate of 94.0% for the easiest situation, Type 1. Even though strawberries were in groups (a challenging situation), the success rate for Type 2 strawberries was 84.48%. Notice that 34.48% of them were picked in the second attempt. This is because the picking motion of the end-effector initially breaks up the groups, separating strawberries and making them easier to pick in a subsequent attempt. It is less likely for them to get covered since they are already isolated. Type 3 closely follows with a success rate of 78.63%, showing that partially covered strawberries are more difficult to harvest. The success rate significantly drops for Types 4 (59.14%) and Type 5 (37.50%). This shows challenges for our harvesting subsystems (vision and picking) in dealing with groups of strawberries that

Fig. 14. Artificial strawberry misclassified due to varying light conditions.

Fig. 15. Diseased/wilted leaves misclassified as mature strawberries.

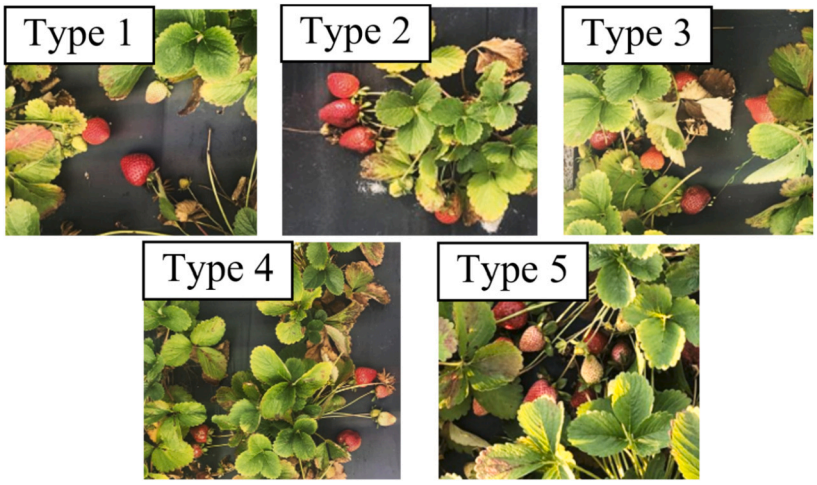

Fig. 16. Strawberry growth situations classification.

are covered by obstacles (e.g., stems and leaves) and in the later stage of a growing season.

The harvesting time was automatically measured by software and was counted from the moment the manipulator leaves its home position until returns to it, including the picking and traveling times. This time corresponds to one attempt per strawberry, and for the cases with more than one reachable fruit, we divided the total time by the number of reachable fruits. For the cases with more than one reachable strawberry, we divided the total time by the number of attempted fruits. Fig. 17 shows an error bar with the maximum, minimum, and average harvesting times as a function of the number of attempted strawberries during both laboratory and field tests. For the laboratory tests, uniformly distributed, random coordinate pairs were generated 300 times for every case of attempted strawberries. The overall average harvesting time was 8.57 s with a maximum of 11.9 s and a minimum of 6.2 s per strawberry. For the field tests, the overall average harvesting time was 7.5 s with a maximum of 11.74 s and a minimum of 5.9 s per strawberry. The gradual decrease in the harvesting time is because the manipulator does not return to the home position after dropping every fruit in the collection basket, but instead it goes straight to the next reachable fruit. The "true" time would be an average of the harvesting times for fruits located at every point in the reachable area (infinite points). The more

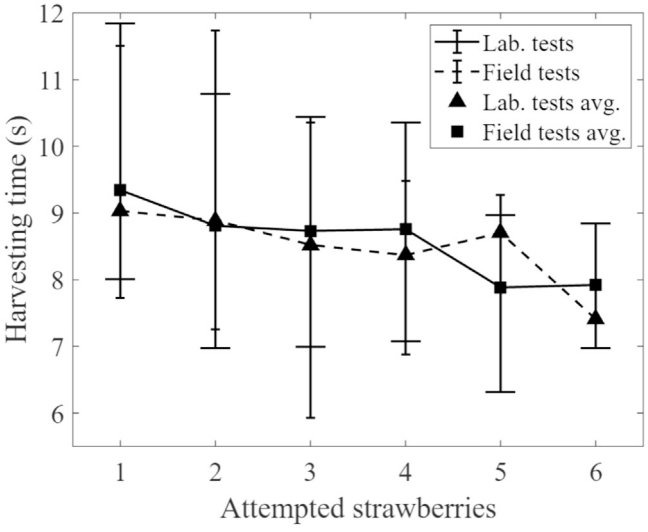

Fig. 17. Harvesting times in both laboratory (solid line, larger cap) and field (dashed line, shorter cap) experiments as a function of the number of reachable strawberries.

Table 4
Performance assessment indicators for the three robotic strawberry harvesters.

	Harvest success rate	Cycling time	# of picked strawberries
Our robot	71.7%	7.5 s	449
Robot in [14]	79.43%	6.1 s	139
Robot in [15]	67.1%	31.5 s	159

points we have, the closer we get to converge to the true value. This trend is seen in Fig. 17. Moreover, the average harvesting time during field experiments was smaller than the time in laboratory experiments in most of the cases. Because of the pattern plants are placed on the beds, strawberries often grow in areas near the center, which is closely aligned with the home position of the arms. Thus, the end-effector travels short distances more often, as opposed to locations near the edges of the bed.

In Table 4, we show a comparison between our platform and other small strawberry harvesting robotic systems found in the literature. We excluded commercial robots from this comparison as detailed data about their performance is not publicly available and they belong to a different category. The table shows two indicators that are generally used to assess the performance of robotic harvesting systems. The harvest success rate is defined as the number of picked mature fruits versus the number of target fruits. The cycling time is the time it takes the robot to harvest a single fruit with a single manipulator/end-effector. This time includes image processing, motion planning, and execution. It is worth noting that the other robots used in this comparison were tested in greenhouses and not in open fields, and the comparison might be unfair to our proposed robot as the growing conditions in open fields are significantly more different and more challenging. Nonetheless, it can provide a general insight into the current state of non-commercial strawberry harvesting systems. The robotic system in [14], with a single-rail dual-arm manipulator, reported harvesting 139 out of 175 strawberries for a 79.43% harvest success rate, and a cycling time of 6.1 s. The 7-DOF robotic arm on a stationary platform in [15] achieved a harvest success of 67.1% by picking 159 out of 237 strawberries, and a cycling time of 31.5 s. Our system, even though does not have the highest harvest success (71.7%), is very fast with a cycling time of 7.5 s. It is also worth noting that our robot has been tested the most with a total of 449 out of 626 strawberries harvested, and furthermore, not all scenarios in our harvesting were experienced by the other robotic harvesters in greenhouses.

On a new test performed on March 21, 2023, we measured the damage rate, defined as the percentage of damaged/bruised fruits during and after the harvesting process. We assume that any damaged fruit is an unsellable fruit, though, they can still be used to create derived products such as jelly. We performed a visual inspection right after each fruit was picked, and then 24 hours afterwards to check for possible bruises caused by the pulling of the fingers. Out of 34 harvested strawberries, only two were slightly bruised or damaged by the end effector for a 5.9% damage rate. We found that bruising happens due to inaccurate height estimation. As the fingers retract, they scratch the fruits without grabbing them. Bruising also occurred to strawberries adjacent to the one attempted. As the end-effector reaches down for a fruit, the tip of the fingers may puncture those near the target. We did not observe any bruising or food quality degradation 24 hours after harvesting.

3.5. Discussion of failure cases during field experiments and future directions

The failure cases in Table 3 are due to the following three reasons. (i) The vision system fails to identify the strawberries in subsequent attempts due to occlusions or varying lighting conditions. (ii) The end-effector is not strong enough to close its fingers when breaking the stem of a strawberry. This happens mostly when the end-effector attempts to grasp a group of strawberries. This is not an issue of the fingers themselves, but of the servomechanism used to close them. (iii) The initial height estimation falls short, and a failed attempt is counted. Subsequent picking attempts can solve this issue, but it could be addressed from the first time by using a more complex height detection approach.

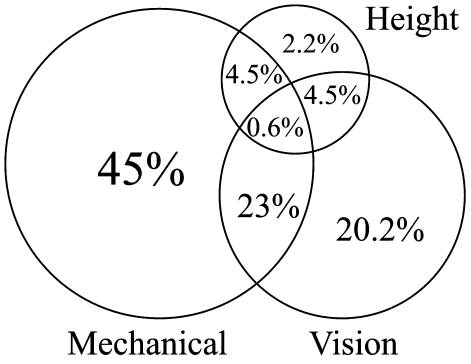

Fig. 18. Percentages of failed cases according to their causes.

In Fig. 18, we can see the distribution between the causes of failure. Out of 177 failed attempts, about 72.9% of them included mechanical reasons whereas 44.6% were mechanical only. Failures that included vision-related limitations accounted for 48.6% of the total, with 20.3% of them being due to vision only. Failed picking attempts for Types 2 to 5 were due to mechanical, vision, or a combination of both reasons. Failed attempts that included height estimation inaccuracy correspond to 11.9% of the total, with 2.3% of them being due to the height estimation issue only. Note that our height estimation strategy does not have a significant impact on the total number of failed cases. Failed attempts for Type 1 strawberries were caused exclusively due to height estimation reasons. Since they are isolated, they are easy to detect and pick; thus, there were no mechanical or vision issues involved.

Future direction 1: More field experiments will be done in different stages of the strawberry growing season in Florida, and failure cases will be analyzed to determine the main issues in the robotic harvesting.

Future direction 2: A stronger servomechanism will be adopted so the fingers can be closed tightly. Also, to avoid bruising picked fruits, a different fruit detachment mechanism, soft materials for the end-effector or a design like in [35] may be adopted.

Future direction 3: A better vision algorithm can be adopted to estimate the center of partially covered strawberries.

Future direction 4: A more complex height estimation method will be implemented that could include the use of an RGB-D sensor or LiDAR. On the other hand, it is noted that in [35] we investigated a method to reliably estimate the Z-coordinate using the in-hand RGB camera of the end-effector. However, the algorithm is out of the scope of this paper and will be considered as another alternative. This would reduce the occurrence of the height estimation as one of the main sources of failure of our system and decrease the damage to the fruits.

Future direction 5: An environmental impact study should be carried out to identify and evaluate the potential effects that our planned fleet of robots would have on farms and on the environment. Such study would provide vital information about the effects of our system in other farming activities such as irrigation, soil fertilization or pesticide delivery; while also considering sustainable practices related to energy efficiency and responsible use of natural resources.

4. Conclusions

In this work, a small harvesting robot is presented to pick strawberries in open field conditions. Three key subsystems, vision, picking, and GNC, are discussed. The deep NN-based vision subsystem implements a YOLOv4 (small objects) model to locate mature strawberries from RGB images with high accuracy. The picking mechanism includes a manipulator in a Delta configuration and a five-finger end-effector. The GNC

subsystem is based on a previously developed disease detection robot and can reliably control the robot to stay over beds using ultrasonic range finders. During field tests, the proposed robotic harvester reached high success rates (94.0% and 84.5%) when picking mostly uncovered strawberries (Types 1 and 2, respectively). The harvesting performance decreased to the lowest success rate of 37.5% when occlusions, obstacles, and strawberry clusters posed difficult circumstances (Type 5) for the end-effector to be able to grab and detach fruits. On average over five different scenarios, the robot achieved a harvest success rate of 71.7% with an average harvest time (cycle time) of 7.5 s per fruit.

CRediT authorship contribution statement

Luis Tituaña: Data curation, Formal analysis, Investigation, Methodology, Software, Validation, Visualization, Writing – original draft. **Akram Gholami:** Data curation, Investigation, Methodology, Software, Writing – original draft. **Zixuan He:** Data curation, Investigation, Methodology, Software, Writing – original draft. **Yunjun Xu:** Conceptualization, Funding acquisition, Investigation, Methodology, Project administration, Resources, Supervision, Writing – review & editing. **Manoj Karkee:** Conceptualization, Funding acquisition, Investigation, Methodology, Project administration, Resources, Supervision, Writing – review & editing. **Reza Ehsani:** Conceptualization, Funding acquisition, Investigation, Methodology, Project administration, Resources, Supervision.

Declaration of competing interest

The authors declare that they have no known competing financial interests or personal relationships that could have appeared to influence the work reported in this paper.

Data availability

The authors are unable or have chosen not to specify which data has been used.

Acknowledgements

This work was supported by the National Science Foundation under Grants No. 1924622, No. 1924640, and No. 1924662. The authors would like to thank Pappy's Patch and BigDaddy's Organic Farm for letting us conduct experiments in their commercial strawberry field.

References

[1] T. Searchinger, R. Waite, C. Hanson, J. Ranganathan, E. Matthews, Creating a sustainable food future: a menu of solutions to feed nearly 10 billion people by 2050, https://www.wri.org/research/creating-sustainable-food-future, jul 2019.
[2] United States Department of Agriculture, 2017 census of agriculture: United States - summary and state data, apr 2019.
[3] D. Charlton, M. Castillo, Potential impacts of a pandemic on the US farm labor market, Appl. Econ. Perspect. Policy 43 (1) (2021) 39–57, https://doi.org/10.1002/aepp.13105.
[4] S. Valle, J. Kienzle, Agriculture 4.0–agricultural robotics and automated equipment for sustainable crop production, Integr. Crop Manag. 24 (2020), https://www.fao.org/documents/card/en/c/CB2186EN.
[5] C.W. Bac, E.J. van Henten, J. Hemming, Y. Edan, Harvesting robots for high-value crops: state-of-the-art review and challenges ahead, J. Field Robot. 31 (6) (2014) 888–911, https://doi.org/10.1002/rob.21525.
[6] C.-L. Chang, K.-M. Lin, Smart agricultural machine with a computer vision-based weeding and variable-rate irrigation scheme, Robotics 7 (3) (2018) 38, https://doi.org/10.3390/robotics7030038.
[7] A.T. Meshram, A.V. Vanalkar, K.B. Kalambe, A.M. Badar, Pesticide spraying robot for precision agriculture: a categorical literature review and future trends, J. Field Robot. 39 (2) (2022) 153–171, https://doi.org/10.1002/rob.22043.
[8] J. Underwood, A. Wendel, B. Schofield, L. McMurray, R. Kimber, Efficient in-field plant phenomics for row-crops with an autonomous ground vehicle, J. Field Robot. 34 (6) (2017) 1061–1083, https://doi.org/10.1002/rob.21728.
[9] X. Wu, S. Aravecchia, P. Lottes, C. Stachniss, C. Pradalier, Robotic weed control using automated weed and crop classification, J. Field Robot. 37 (2) (2020) 322–340, https://doi.org/10.1002/rob.21938.
[10] T. Botterill, S. Paulin, R. Green, S. Williams, J. Lin, V. Saxton, S. Mills, X. Chen, S. Corbett-Davies, A robot system for pruning grape vines, J. Field Robot. 34 (6) (2017) 1100–1122, https://doi.org/10.1002/rob.21680.
[11] S.G. Defterli, Y. Shi, Y. Xu, R. Ehsani, Review of robotic technology for strawberry production, Appl. Eng. Agric. 32 (3) (2016) 301–318, https://doi.org/10.13031/aea.32.11318.
[12] Y. Nagasaki, S. Hayashi, Y. Nakamoto, H. Kawashima, Y. Kohno, Development of a table-top cultivation system for robot strawberry harvesting, Jpn. Agric. Res. Q., JARQ 47 (2) (2013) 165–169, https://doi.org/10.6090/jarq.47.165.
[13] Y. Xiong, C. Peng, L. Grimstad, P.J. From, V. Isler, Development and field evaluation of a strawberry harvesting robot with a cable-driven gripper, Comput. Electron. Agric. 157 (2019) 392–402, https://doi.org/10.1016/j.compag.2019.01.009.
[14] Y. Xiong, Y. Ge, L. Grimstad, P.J. From, An autonomous strawberry-harvesting robot: design, development, integration, and field evaluation, J. Field Robot. 37 (2) (2020) 202–224, https://doi.org/10.1002/rob.21889.
[15] S. Yamamoto, S. Hayashi, H. Yoshida, K. Kobayashi, Development of a stationary robotic strawberry harvester with a picking mechanism that approaches the target fruit from below, Jpn. Agric. Res. Q., JARQ 48 (3) (2014) 261–269, https://doi.org/10.6090/jarq.48.261.
[16] Octinion, Rubion, http://octinion.com/products/agricultural-robotics/rubion, 2022. (Accessed 30 June 2022).
[17] Y. Chen, W.S. Lee, H. Gan, N. Peres, C. Fraisse, Y. Zhang, Y. He, Strawberry yield prediction based on a deep neural network using high-resolution aerial orthoimages, Remote Sens. 11 (13) (2019) 1584, https://doi.org/10.3390/rs11131584.
[18] P. Menendez-Aponte, X. Kong, Y. Xu, An approximated, control affine model for a strawberry field scouting robot considering wheel–terrain interaction, Robotica 37 (9) (2019) 1545–1561, https://doi.org/10.1017/S0263574719000134.
[19] Agrobot, Agrobot, https://www.agrobot.com/e-series, 2022. (Accessed 30 June 2022).
[20] Harvest CROO Robotics, Technology, https://www.harvestcroorobotics.com/technology, 2022. (Accessed 30 June 2022).
[21] Advanced Farm Technologies, Strawberry harvester, https://advanced.farm/technology/strawberry-harvester/, 2022. (Accessed 5 September 2022).
[22] Traptic, Traptic, https://www.traptic.com/, 2022. (Accessed 12 April 2022).
[23] Naber's Ag Equipment LLC., Easypick™ harvest assistant, http://www.nabersequipment.com/2.html, 2022. (Accessed 12 April 2022).
[24] AgPro Robotics, Products—AgPro robotics, http://www.agprorobotics.com/products, 2022. (Accessed 12 April 2022).
[25] D. Freese, Y. Xu, Nonlinear robust path control for a field robot scouting in strawberry orchards, in: ASME Dyn. Syst. and Control Conf., 2017, DSCC2017-5220.
[26] F. Khosro Anjom, S.G. Vougioukas, D.C. Slaughter, Development and application of a strawberry yield-monitoring picking cart, Comput. Electron. Agric. 155 (2018) 400–411, https://doi.org/10.1016/j.compag.2018.10.038.
[27] Q. Li, X. Kong, Y. Xu, Marker based row alignment control for an agricultural scouting robot, in: ASME Dyn. Syst. Control Conf., 2020, DSCC2020-3183.
[28] Q. Li, Y. Xu, Minimum-time row transition control of a vision-guided agricultural robot, J. Field Robot. 39 (4) (2021) 335–354, https://doi.org/10.1002/rob.22053.
[29] D.J. Freese, Y. Xu, Multiphase scouting control of an agricultural field robot with reachability analyses, J. Dyn. Syst. Meas. Control 141 (5) (2019) 051009, https://doi.org/10.1115/1.4041850.
[30] P. Menendez-Aponte, C. Garcia, D. Freese, S. Defterli, Y. Xu, Software and hardware architectures in cooperative aerial and ground robots for agricultural disease detection, in: 2016 Int. Conf. Collab. Technol. Syst. (CTS), 2016, pp. 354–358.
[31] F. Dimeas, D.V. Sako, V.C. Moulianitis, N.A. Aspragathos, Design and fuzzy control of a robotic gripper for efficient strawberry harvesting, Robotica 33 (5) (2015) 1085–1098, https://doi.org/10.1017/S0263574714001155.
[32] B. Zhang, Y. Xie, J. Zhou, K. Wang, Z. Zhang, State-of-the-art robotic grippers, grasping and control strategies, as well as their applications in agricultural robots: a review, Comput. Electron. Agric. 177 (2020) 105694, https://doi.org/10.1016/j.compag.2020.105694.
[33] N. Kondo, K. Ninomiya, S. Hayashi, T. Ota, K. Kubota, A new challenge of robot for harvesting strawberry grown on table top culture, in: 2005 ASAE Annu. Int. Meet., 2005, 053138.
[34] S. Hayashi, K. Shigematsu, S. Yamamoto, K. Kobayashi, Y. Kohno, J. Kamata, M. Kurita, Evaluation of a strawberry-harvesting robot in a field test, Biosyst. Eng. 105 (2) (2010) 160–171, https://doi.org/10.1016/j.biosystemseng.2009.09.011.
[35] J. Mapes, A. Dai, Y. Xu, S. Agehara, Harvesting end-effector design and picking control, in: 2021 IEEE Symp. Ser. Comput. Intell. (SSCI), 2021, pp. 01–06.
[36] R. Fernandez, H. Montes, J. Surdilovic, D. Surdilovic, P. Gonzalez-De-Santos, M. Armada, Automatic detection of field-grown cucumbers for robotic harvesting, IEEE Access 6 (2018) 35512–35527, https://doi.org/10.1109/ACCESS.2018.2851376.
[37] J.-Y. Choi, K. Seo, J.-S. Cho, K.-D. Moon, Applying convolutional neural networks to assess the external quality of strawberries, J. Food Compos. Anal. 102 (2021) 104071, https://doi.org/10.1016/j.jfca.2021.104071.
[38] Y. Yu, K. Zhang, L. Yang, D. Zhang, Fruit detection for strawberry harvesting robot in non-structural environment based on Mask-RCNN, Comput. Electron. Agric. 163 (2019) 104846, https://doi.org/10.1016/j.compag.2019.06.001.
[39] A. Bochkovskiy, C.-Y. Wang, H.-Y. Liao, YOLOv4: optimal speed and accuracy of object detection, arXiv:2004.10934, 2020, https://doi.org/10.48550/arXiv.2004.10934.

[40] J. Redmon, A. Farhadi, YOLO9000: better, faster, stronger, in: 2017 IEEE Conf. Comput. Vision Pattern Recognit. (CVPR), 2017, pp. 6517–6525.
[41] Y. Yu, K. Zhang, H. Liu, L. Yang, D. Zhang, Real-time visual localization of the picking points for a ridge-planting strawberry harvesting robot, IEEE Access 8 (2020) 116556–116568, https://doi.org/10.1109/ACCESS.2020.3003034.
[42] K. He, X. Zhang, S. Ren, J. Sun, Spatial pyramid pooling in deep convolutional networks for visual recognition, IEEE Trans. Pattern Anal. Mach. Intell. 37 (9) (2015) 1904–1916, https://doi.org/10.1109/TPAMI.2015.2389824.
[43] S. Liu, L. Qi, H. Qin, J. Shi, J. Jia, Path aggregation network for instance segmentation, in: 2018 IEEE/CVF Conf. Comput. Vision Pattern Recognit., 2018, pp. 8759–8768.
[44] Z. He, M. Karkee, P. Upadhayay, Detection of strawberries with varying maturity levels for robotic harvesting using YOLOv4, in: 2021 ASABE Annu. Int. Virtual Meet., 2021, 2100051.
[45] M. Mapes, Y. Xu, Row allocation negotiation for a fleet of strawberry harvesting robots, ASME Lett. Dyn. Syst. Control 2 (3) (2022) 031007, https://doi.org/10.1115/1.4054644.
[46] Y. Zhang, J. Yu, Y. Chen, W. Yang, W. Zhang, Y. He, Real-time strawberry detection using deep neural networks on embedded system (rtsd-net): an edge AI application, Comput. Electron. Agric. 192 (2022) 106586, https://doi.org/10.1016/j.compag.2021.106586.
[47] Tzutalin, LabelImg [Online], https://github.com/tzutalin/labelImg, 2022. (Accessed 2022).
[48] Alexey, Yolo v4, v3 and v2 for Windows and Linux [Online], https://github.com/AlexeyAB/darknet, 2022. (Accessed 2022).
[49] L. Fu, F. Gao, J. Wu, R. Li, M. Karkee, Q. Zhang, Application of consumer RGB-D cameras for fruit detection and localization in field: a critical review, Comput. Electron. Agric. 177 (2020) 105687, https://doi.org/10.1016/j.compag.2020.105687.
[50] M. López, E. Castillo, G. García, A. Bashir, Delta robot: inverse, direct, and intermediate Jacobians, Proc. Inst. Mech. Eng., Part C, J. Mech. Eng. Sci. 220 (1) (2006) 103–109, https://doi.org/10.1243/095440606X78263.
[51] J. Brinker, B. Corves, Y. Takeda, Kinematic and dynamic dimensional synthesis of extended delta parallel robots, in: Robotics Mechatron., Springer International Publishing, 2019, pp. 131–143.
[52] M. Mahmoodi, M.G. Tabrizi, K. Alipour, A new approach for kinematics-based design of 3-RRR delta robots with a specified workspace, in: 2015 AI & Robotics (IRANOPEN), 2015, pp. 1–6.
[53] J. Davidson, S. Bhusal, C. Mo, M. Karkee, Q. Zhang, Robotic manipulation for specialty crop harvesting: a review of manipulator and end-effector technologies, Glob. J. Agric. Allied Sci. 2 (1) (2020) 25–41, https://doi.org/10.35251/gjaas.2020.004.
[54] Y. Xiong, Y. Ge, Y. Liang, S. Blackmore, Development of a prototype robot and fast path-planning algorithm for static laser weeding, Comput. Electron. Agric. 142 (2017) 494–503, https://doi.org/10.1016/j.compag.2017.11.023.
[55] J. Lee, H.-J. Cho, B. Choi, J. Sung, S. Lee, M. Shin, Life cycle assessment of tractors, Int. J. Life Cycle Assess. 5 (4) (2000) 205–208, https://doi.org/10.1007/BF02979361.